Summary

Bacteria adapt to elevated levels of Reactive Oxygen Species (ROS) by increasing the expression of defence and repair proteins, which is regulated by ROS responsive transcription factors. In *Bacillus subtilis* the zinc protein PerR, a peroxide sensor that binds DNA in the presence of a regulatory metal Mn^{2+} or Fe^{2+}, mediates the adaptive response to H_2O_2. This study presents the first crystal structure of apo-PerR-Zn which shows that all four cysteine residues of the protein are involved in zinc co-ordination. The $Zn(Cys)_4$ site locks the dimerization domain and stabilizes the dimer. Sequence alignment of PerR-like proteins supports that this structural site may constitute a distinctive feature of this class of peroxide stress regulators.

Introduction

Oxidative stress is generated by exposure to elevated levels of Reactive Oxygen Species (ROS), such as superoxide anion, hydrogen peroxide and the highly toxic hydroxyl radical which can damage proteins, nucleic acids and cell membranes (Storz and Imlay, 1999). To avoid or counter the harmful effects of ROS, cells constitutively express proteins to protect themselves and repair the damages. These proteins are under negative control of specific regulators which are the central pieces of the adaptive and inducible responses to oxidative stress present in cells (Mongkolsuk and Helmann, 2002). These regulators sense the increase of ROS and transduce the signal into increased expression of defence activities. Among the best-understood regulators of oxidative stress responses in bacteria is OxyR which is the hydrogen peroxide sensor in *Escherichia coli*. The OxyR regulon includes genes involved in peroxide metabolism and protection (*katG*, *ahpCF*, *dps*), redox balance (*gorA*, *grxA*, *trxC*) and important regulators such as *fur* and *oxyS* RNA (Zheng *et al*., 2001a,b). From thorough crystallographic and biochemical analyses, Storz and coworkers (Zheng *et al*., 1998) have proposed a mechanism based on a H_2O_2-induced thiol–disulphide switch (Choi *et al*., 2001). However, The Stamler group has given a different picture for the activation of OxyR. Kim *et al*. (2002) find no evidence for an intramolecular disulphide bond but instead demonstrate that Cys-199 of OxyR can undergo different stable chemical modifications in response to oxidative or nitrosative stress. These authors have shown that these modifications affect OxyR DNA binding *in vitro* and suggested that distinct chemical modifications will lead to fine tuning of OxyR activity.

Bacillus subtilis displays an adaptive response to hydrogen peroxide. In this Gram-positive bacteria, the metalloprotein PerR was identified in Helmann's laboratory as a member of the Fur (Ferric uptake regulator) family (Mongkolsuk and Helmann, 2002). PerR is the major regulator of the peroxide stress response, a property that makes it functionally analogous to OxyR. Insight into the mechanism controlling the peroxide stress response in *B. subtilis* emerged from analysis of *mrgA* regulation. This gene encodes a protective DNA binding protein which is a Dps homologue (Chen and Helmann, 1995; Chen *et al*., 1995). It was initially demonstrated that expression of *mrgA* is subjected to metal regulation. The *mrgA* gene repression, elicited by growth with either added manganese or iron (Chen *et al*., 1993), is mediated by PerR (Bsat *et al*., 1998). The *B. subtilis* PerR regulon includes genes coding for MrgA, the major vegetative catalase (KatA), an alkyl hydroperoxide reductase (AhpCF), haem biosynthesis enzymes (HemAXCDBL), a Zn^{2+} uptake P-type ATPase (ZosA), PerR and Fur (Fuangthong *et al*., 2002). Like other Fur-like homologues, PerR is a small dimeric protein which contains two metal ions per monomer (Herbig andHelmann, 2001). One of the metal binding sites co-ordinates a zinc ion that is generally assigned a structural role, whereas the second site binds a regulatory metal required for DNA binding. *In vivo*, there is evidence that PerR can exist in two metallated forms, PerR-Zn-Fe and PerR-Zn-Mn, where either Fe^{2+} or Mn^{2+} functions as corepressor of gene expression. It was shown that H_2O_2 induces PerR dissociation from DNA. However, these two forms of PerR differ dramatically in their response to hydrogen peroxide. In Mn^{2+}-added medium

the PerR regulon is strongly repressed and peroxide induction is inefficient. In contrast, with Fe^{2+}-supplemented medium, peroxide induction is maximal and comparable with that of *perR* null mutant strains (Herbig and Helmann, 2001; Fuangthong *et al*., 2002). PerR and PerR-like regulators have been identified in a wide variety of organisms including *Campylobacter jejuni* (van Vliet *et al*., 1999), *Streptomyces reticuli* (Ortiz de Orué Lucana and Schrempf, 2000), *Streptomyces coelicolor* (Hahn *et al*., 2000), *Streptococcus pyogenes* (King *et al*., 2000), *Staphylococcus aureus* (Horsburgh *et al*., 2001) and *Borrelia burgdorferi* (Boylan *et al*., 2003).

Concerning the activation of PerR by H_2O_2, several hypotheses were first advanced (Herbig and Helmann, 2001; Mongkolsuk and Helmann, 2002). However, very recently, Lee and Helmann (2006) reported that PerR senses H_2O_2 by metal-catalysed histidine oxidation. PerR oxidation, mediated by a bound ferrous ion, leads to the incorporation of one oxygen atom into His-37 or His-91, two of the residues that are supposed to co-ordinate the bound Fe^{2+}. This oxidation would lead to iron release and dissociation of the PerR DNA adduct. The proposed mechanism relies on the reduction of H_2O_2 by Fe^{2+} and the generation of highly reactive hydroxyl radicals (Fenton reaction). By analogy to metal-catalysed oxidative reactions with histidine-containing enzymes and model peptides (Schoneich, 2000; Uchida and Kawakishi, 1993; 1994), the authors propose that the hydroxyl radical reacts with histidine and generates the 2-oxo-histidinyl radical intermediate which finally leads to the 2-oxo-histidine.

In this report we present the crystal structure of *B. subtilis* apo-PerR-Zn (PerR-Zn). To our knowledge this is the first structure of a metalloprotein involved in the inducible peroxide stress response. Interestingly, the zinc ion of PerR-Zn is co-ordinated by the four cysteine residues of the protein. The $Zn(Cys)_4$ site plays a crucial role in the stability of the protein by locking the dimerization domain. Molecular modelling of the present PerR-Zn structure allows us to propose a model for the active form of PerR. Moreover, taking advantage of the latter model and the sequence alignment of more than twenty PerR-like proteins we have been able to identify a potential binding site for the regulatory metal.

Results

Purification, metal content analysis and DNA binding

PerR was overexpressed in *E. coli* and purified to homogeneity using a two-step protocol adapted from Herbig and Helmann (2001) (see *Experimental procedures* and Fig. S1 for details). Electrospray ionisation mass spectrometry, under denaturing conditions, indicated an m/z of 16 291.5 (±2.0) Da that corresponds to the expected mass with the missing first methionine residue (calculated m/z for the monomer = 16 292.5 Da). Metal content analysis was carried out by atomic absorption spectroscopy using purified PerR samples that were exchanged into Chelex-100-treated Tris-HCl buffer. The results indicate that zinc is present at a ratio of 0.8 (±0.15) mol of zinc per mol of PerR monomer. Through all preparations of PerR samples, iron and manganese were only detected in trace amounts. Our purification protocol leads exclusively to one form of PerR which retains a single zinc ion per monomer (PerR-Zn). When using Chelex-treated buffers for electrophoretic mobility shift assays, PerR-Zn was inactive and did not bind a DNA fragment containing the PerR box from the *mrgA* promoter. However, upon addition of 1.5 eq. of Mn^{2+} to PerR-Zn, we have been able to reconstitute an active PerR-Zn-Mn protein which binds the *mrgA* PerR box (Fig. S2).

Overall structure of PerR-Zn

The crystal structure of PerR-Zn protein was determined by multiwavelength anomalous diffraction (MAD) and refined to 1.75 Å at the zinc K edge (Table 1). The protein is a

homodimer of 144-amino-acid residues (the initial methionine residue is missing). The asymmetric unit of the crystal contains two monomers related by a non-crystallographic twofold axis. Each monomer is composed of two domains, an N-terminal domain (residues 2–85, shown in red for monomer A in Fig. 1) containing the DNA binding motif and a C-terminal domain (residues 92–144, in orange for monomer A in Fig. 1) involved in the dimerization of the protein. The two domains are connected by a loop (residues 86–91). The N-terminal domain is composed of four α-helices (H1–H4) followed by a two-stranded anti-parallel β-sheet (S1, S2). The DNA binding domain of *Bs*-PerR-Zn was identified by structure superposition with other regulators including *Pseudomonas aeruginosa*-Fur (*Pa*-Fur) (Pohl *et al*., 2003), *Corynebacterium diphtheriae*-DtxR (*Cd*-DtxR) (Pohl *et al*., 1998), and *Mycobacterium tuberculosis*-IdeR (*Mt*-IdeR) (Pohl *et al*., 1999a). As illustrated in Fig. S3, all four proteins share the same basic fold with the typical helix–turn–helix (H3–T–H4) motif which contains the putative DNA binding helix H4 (Val-56 to Ser-69 for *Bs*-PerR-Zn). As reported by Huffman and Brennan (2002), a third helix (H2) may stabilize the helix–turn–helix motif as a compact globular domain. In addition, *Bs*-PerR-Zn and *Pa*-Fur (Pohl *et al*., 2003) contain an additional N-terminal helix H1 (residues 5–15 for *Bs*-PerR-Zn and residues 2–9 for *Pa*-Fur) that may be involved in DNA recognition. The C-terminal part of each PerR-Zn monomer (Fig. 1) consists of a α/β domain with three anti-parallel β-strands (S3, S4 and S5) and two α-helices (H5, H6).

Table 1. Crystallographic data and refinement statistics.

	Data collection		
Space group	P1		
Cell dimensions			
a, *b*, *c* (Å)	40.8, 41.6, 53.9		
α, β, γ (°)	82.2, 80.1, 60.9		
	Peak	***Inflection***	***Remote***
Wavelength	1.2824	1.2828	0.9763
Resolution (Å)	30-2.0	30-2.0	30-1.75
R_{merge}	3.6 (17.1)	3.4 (17.6)	4.5 (26.6)
I /σI	12.5 (5.3)	12.8 (4.8)	12.7 (3.7)
Completeness (%)	81.8 (40.8)	85.5 (42.6)	93.3 (87.2)
Redundancy	1.2	1.2	2.4

Refinement

1. The values in parenthesis are for the highest resolution bin.
2. $R_{merge} = R_{work} = \Sigma_h\Sigma_i|I_{hi} - \langle I_h\rangle|/\Sigma_h\Sigma_i I_{hi}$, were I_{hi} is the *i*th observation of the reflection h, while $\langle I_h\rangle$ is the mean intensity of reflection h.
3. $R_{factor} = \Sigma||F_o| - |F_c||/|F_o|$. R_{free} was calculated with a small fraction (5%) of randomly selected reflections.
4. The Rfree was calculated from 5% of all data that were not used in the refinement.

Resolution (Å)	35.37-1.75
No. reflections	28 332
R_{work}/R_{free}	18.0/23.0
No. atoms	2566
Protein	2275
Ligand/ion	2
Water	289

Refinement

B-factors	
Protein	29.97
R.m.s. deviations	
Bond lengths (Å)	0.012
Bond angles (°)	1.261

Figure 1. Ribbon representation of the PerR-Zn dimer crystal structure. Secondary structure elements are annotated in the drawing. View along the non-crystallographic twofold axis. N-terminal and C-terminal domains of monomer A are in red and orange respectively. N-terminal and C-terminal domains of monomer B are in green and light green respectively.

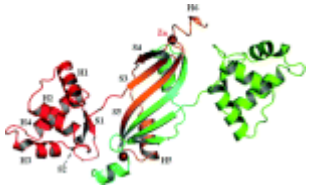

Structure of the zinc binding site

The present data clearly show that one zinc ion is present per monomer and that all four cysteine residues of each monomer are involved in the Zn^{2+} co-ordination. The Zn^{2+} ion is co-ordinated in a tetrahedral fashion with the Zn-S distances ranging from 2.32 Å to 2.36 Å (Fig. 2). As a value of 2.31 Å is expected for a thiolate-Zn^{2+} distance (Simonson and Calimet, 2002), in *Bs*-PerR-Zn the zinc ion is most likely co-ordinated by four thiolates. This zinc binding site, located in the C-terminal domain, consists of two Cys-$(Xaa)_2$-Cys motifs involving Cys-96, Cys-99 and Cys-136, Cys-139 respectively. The two motifs are connected by a 36-residue-long oligopeptide. Cys-96 is the last residue of the S3 β-strand, while Cys-99 is located on the hairpin between the two S3 and S4 β-strands. Following the polypeptide chain to the C-terminal end, Cys-136 is located in the short coil between the S5 β-strand and the H6 α-helix, while Cys-139 belongs to H6 helix. The tertiary fold of the protein brings the three S3, S4 and S5 β-strands in close proximity so as to form a β-sheet and this arrangement is locked by the zinc binding site (Fig. 2). As the latter three β-strands are part of the dimerization domain, the zinc ion appears to play a crucial structural role in maintaining the stability of the dimer.

Figure 2. Zinc binding site and dimerization domain of PerR-Zn. Close-up of the dimerization domain and the zinc binding site of PerR-Zn (monomer A). S3-5 β-strands, H6 helix and the zinc ion are annotated. Metal to cysteine ligand distances are 2.36, 2.31, 2.31 and 2.32 Å for Cys-96, Cys-99, Cys-136, Cys-139 respectively.

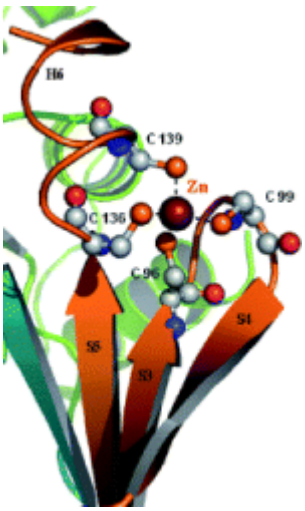

Role of the zinc site in the stability of the dimer

To check whether the $Zn(Cys)_4$ centre of PerR-Zn plays a structural role, oxidative reactions were performed with H_2O_2 and diamide, a thiol-specific oxidant. Oxidation of the protein was then evaluated by FPLC using a gel filtration column. For these experiments, all buffers were Chelex-treated to avoid any potential Fenton-like reactions which could damage the protein. The dimeric form of PerR elutes as a single peak with an elution volume of 10 ml (Fig. 3 insert). Oxidative treatment with either H_2O_2 or diamide leads to two new products, **II** and **III** (a typical profile of these reactions is shown in Fig. 3). The elution volumes observed for **II** (11.5 ml) and **III** (7.5 ml) suggest a monomeric and an oligomeric form of the protein respectively. It must be noted that the formation of **III** is prevented in the presence of a high ionic strength (0.5 M NaCl). Electrospray mass spectrometry analysis of **II**, obtained with either H_2O_2 or diamide treatment, led to an m/z of 16 287.5 (±2.0) Da which corresponds to the mass of the oxidized monomer. Interestingly, the latter mass value suggests that two disulphide bonds are formed upon oxidative treatment of PerR-Zn. Importantly, metal content analysis by flame atomic absorption revealed that zinc is not present in the oxidized monomer.

Figure 3. Typical FPLC profile for the reaction of PerR-Zn with H_2O_2. Oxidation of PerR-Zn (20 µM) was carried out for 30 min at 37°C, in 100 mM Tris-HCl pH 8, 100 mM NaCl solution, in the presence of 100 eq. H_2O_2. Analysis of the reaction was performed on a gel filtration Superdex-75 column. I, II and III are the dimer, monomer and oligomer species respectively. The profile of the starting dimeric protein is shown in insert.

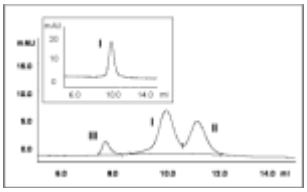

To assess the decomposition rate constant of PerR-Zn under oxidative conditions, the fractional amount of the dimer was plotted in Fig. 4 as a function of time exposure to H_2O_2 or diamide. The concentration of the unreacted dimer was determined by evaluating the area under the peak in the FPLC chromatogram. The experimental points represent the average of at least three separate experiments. The dimer decomposition rate constant was calculated by fitting the experimental data to the monoexponential decay function: $Y = Y_0 + Ae^{(-kt)}$, where k is the decomposition rate constant. The calculated *k*-values for the reaction of PerR-Zn with either H_2O_2 or diamide are 0.96 (±0.12) and 1.08 (±0.12) h^{-1} respectively. Both values are within experimental errors, which suggest that the oxidation of the protein with H_2O_2 and diamide proceed similarly. Oxidation of

the $Zn(Cys)_4$ site was then examined by titration of free thiols with DTNB in the presence of H_2O_2. Figure 5 shows the percentage of thiols titrated with DTNB versus time exposure to H_2O_2 of PerR-Zn. As shown, more than 80% of the thiols are oxidized within 25 min with an estimated rate constant of 0.24 (±0.01) min^{-1}. This result confirms that the oxidized monomer species contains two disulphide bonds in agreement with the mass spectrometry analysis. Altogether these results demonstrate that the zinc ion in PerR-Zn plays a largely structural role because its loss upon oxidation of the four cysteine residues leads to the unfolding of the dimer.

Figure 4. Determination of the PerR-Zn dimer decomposition rate constant upon oxidative treatment. The fractional amount of dimeric protein (PerR-Zn) is plotted as a function of time of exposure to oxidant (H_2O_2 or diamide). The apparent rate constant for the decomposition of the dimer was estimated by fitting the experimental data with a one-phase exponential decay function.

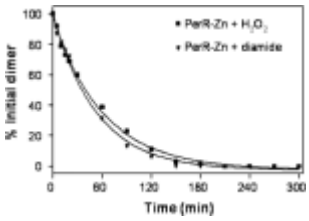

Figure 5. Free thiol titration with DTNB. The percentage of free thiols is plotted as a function of time of exposure of PerR-Zn to H_2O_2. The apparent rate constant for the oxidation of the $Zn(Cys)_4$ site was estimated by fitting the experimental data with a one-phase exponential decay function.

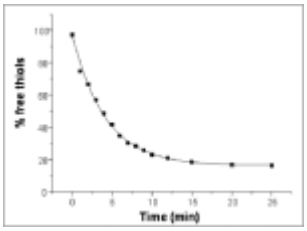

Discussion

Overall structure

The present study provides the first structural description of a Fur-like metalloregulator, PerR from *B. subtilis*, involved in the regulation of the inducible peroxide stress response. Until now, the only structural information on a Fur protein, offered by Pohl *et al.* (2003), describes the structure of the Fur from *P. aeruginosa*. This work revealed significant similarities with related iron-dependent regulators, DtxR from *C. diphtheriae* (Pohl *et al.*, 1998, 1999b) and IdeR from *M. tuberculosis* (Pohl *et al.*, 1999a). Although there is only 26% sequence homology between *Pa*-Fur and *Bs*-PerR, the two proteins present structural similarities notably in the DNA-binding and the dimerization domains. Superposition of *Pa*-Fur and *Bs*-PerR-Zn N-terminal domains leads to an r.m.s. deviation of 1.41 Å (Fig. S3). Furthermore, the two putative DNA binding helices H4 of both regulators superimpose well with an r.m.s. deviation of 0.27 Å. Such a high structural similarity is also found for the α/β dimerization domain of both proteins. The 44 structurally equivalent C_α-atoms of strands S3, S4, S5 and helix H5, superimpose with an r.m.s.d. of 2.6 Å (Fig. S4).

PerR contains a $Zn(Cys)_4$ structural motif

The most striking structural difference between *Bs*-PerR-Zn and *Pa*-Fur resides in the zinc binding site. Indeed, as revealed by the present study, the zinc ion in PerR is bound by four cysteinates. By contrast, in the reported structure of *Pa*-Fur, two histidine (His-32, His-89) and two glutamate (Glu-80, Glu-100) residues co-ordinate the zinc ion (Pohl *et al*., 2003). It is noteworthy that *Pa*-Fur is an exception within the Fur family because it lacks the Cys-95 and therefore the zinc avid Cys-$(Xaa)_2$-Cys motif (involving Cys-92, Cys-95 in *Ec*-Fur notation) which is found in most Fur proteins. Previous work in our laboratory has shown that this motif is indeed involved in zinc binding in *Ec*-Fur, the zinc co-ordination being complemented probably by two histidines residues (Jacquamet *et al*., 1998; Gonzalez de Peredo *et al*., 1999). Therefore, the two other cysteines of *Ec*-Fur protein which belong to a Cys-$(Xaa)_4$-Cys motif (involving Cys-132, Cys-137 in *Ec*-Fur notation and conserved in many Fur proteins from various origins) are not involved in metal binding. The present study has revealed that the $Zn(Cys)_4$ site in PerR-Zn locks together the three S3, S4 and S5 β-strands of each monomer to form the two parts of the dimer β-sheet. The importance of this structural role was confirmed through oxidation of the four cysteine residues which leads to the formation of two disulphide bonds, the zinc release and after all to the dimer disruption (Figs 3–5). Interestingly, sequence alignments of twenty PerR-like proteins from a wide variety of microorganisms reveal that the four cysteine residues are absolutely conserved and strictly organized as two Cys-$(Xaa)_2$-Cys motifs (Fig. S5, with Cys-96, Cys-99 and Cys-136, Cys-139 for *Bs*-PerR). Owing to the present structural results and the well-documented zinc avidity of the Cys-$(Xaa)_2$-Cys motif, it is likely that all these proteins contain a structural $Zn(Cys)_4$ site which may then appear as a distinctive feature of the PerR-like metalloregulators.

A model for the active form of PerR

In spite of the structural homologies between *Pa*-Fur and *Bs*-PerR, the overall dimer structures are different. This is illustrated in Fig. 6, where the superposition of the two central α/β motifs of both proteins leads to a divergent orientation of the two respective DNA-binding motifs. The relative orientation on opposite sides of the two H4 and H4′ helices of PerR-Zn (in red in Fig. 6), forced by the nearly flat structure of the protein, clearly shows that PerR-Zn cannot interact with DNA. In contrast, the structure of active *Pa*-Fur brings together the two putative DNA-binding helices H4 and H4′ with an almost perpendicular orientation which allows their interaction with DNA (in green in Fig. 6) (Pohl *et al*., 2003). A crucial point to address is how the present PerR-Zn structure can account for the structure of the active protein which interacts with DNA upon binding the regulatory metal. Towards this goal, we built a model for the active PerR protein (Fig. 7A). The DALI algorithm [structural comparisons based on Distance matrix ALIgnment (Holm and Sander, 1996)] was used to perform structural comparisons between PerR-Zn and the available structures in the Protein Data Bank (PDB). The closest homologue of PerR-Zn was found to be *Pa*-Fur (Z-score of 13). As already mentioned, the similarities between both proteins are particularly located in the N-terminal domains (residues 1–88) with a Z-score of 13 and an r.m.s.d. of 1.4 Å for the 82 common C_α-atoms. The C-terminal domain of PerR-Zn (residues 89–144) was then compared separately with all protein folds in the PDB using DALI. Interestingly, only the *Pa*-Fur structure showed a Z-score value greater than 4.5. According to these two DALI hits the structural analysis by superposition of both independent domains of *Bs*-PerR-Zn with *Pa*-Fur leads to a model of the active PerR protein. This new model differs from PerR-Zn by a 160° rotation of the C-terminal domain towards the N-terminal end, and leads to a Z-score of 14.5 with an r.m.s.d. of 2.4 Å for the 130 common residues with *Pa*-Fur (Fig. S6). Interestingly the modelled PerR structure reveals that five residues (His-37, His-91, His-93, Asp-85 and Asp-104), conserved among the PerR-like family members (Fig. S5), are suitably located and are thus likely to form a high affinity binding site for the regulatory metal (Fig. 7B). This potential regulatory metal site is consistent with the recent results reported by Lee and Helmann (2006)

who indicated through mutational analyses that the latter five residues proposed to be Fe^{2+} or Mn^{2+} ligands are essential for the repressor function of PerR *in vivo*.

Figure 6. Superposition of *Bs*-PerR-Zn and *Pa*-Fur. Comparison of the global dimer structure of *Bs*-PerR-Zn (orange with H4 helices in red) and *Pa*-Fur (blue with H4 helices in green) using the dimerization domains as the superposition matrix.

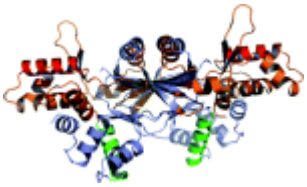

Figure 7. Structural model of the active PerR protein. A. Ribbon representation of the PerR dimer with the two putative DNA binding helices in red. The two zinc atoms are in brown. The five residues of the potential regulatory metal binding site are indicated. B. Close-up of the regulatory metal binding site.

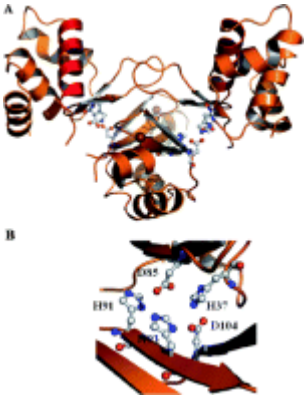

By providing a five donor binding site PerR might have a strong affinity for Fe^{2+}. Moreover, it is noteworthy that among the five ligands, four belong to the C-terminus while one (His-37) belongs to the N-terminal domain of the protein. Therefore, the binding of His-37 onto the iron brings the N- and C-termini in close proximity so that the protein wraps around the regulatory metal which locks together the N- and C-terminal domains to allow for DNA binding. Conversely, peroxide oxidation of His-37 may abolish its iron binding ability and its dissociation from the metal would disrupt the DNA binding form of PerR that would adopt a relaxed structure similar to the presently reported PerR-Zn form.

Conclusion

A few zinc cysteinate redox switches have been described in the recent past and associated to a wide range of biological functions, many of them related to the oxidative and the disulphide stress defences (Paget and Buttner, 2003; Barford, 2004). One of the best-characterized examples is the heat shock protein Hsp33 that behaves as a molecular chaperone and is activated in response to a redox stress. Jakob and coworkers showed that the reduced Hsp33 monomer contains a $Zn(Cys)_4$ site which releases the Zn^{2+} ion upon oxidation and consequently forms the oxidized dimer which is the active form of the chaperone (Jakob *et al*., 1999; 2000; Barbirz *et al*., 2000; Graumann *et al*., 2001). In the case of the peroxide sensor PerR we have shown that the $Zn(Cys)_4$ site is oxidized in the presence of millimolar concentrations of H_2O_2, a level well above that needed to inactivate the PerR-Zn-Fe protein. Thus it is unlikely that oxidation of the $Zn(Cys)_4$ site would contribute, *in vivo*, to the inactivation of the protein and the subsequent induction of the peroxide stress response. In the case of an excess of Mn^{2+}, as PerR-Zn-Mn is

much less sensitive to H_2O_2 than PerR-Zn-Fe, oxidation of the zinc binding site may contribute to Per-Zn-Mn inactivation under strong oxidative conditions. However, this hypothesis requires confirmation *in vivo*.

In summary, the present study has demonstrated that *B. subtilis* PerR possesses a $Zn(Cys)_4$ site which is crucial to stabilize the dimeric form of the protein. Sequence homologies of twenty PerR and PerR-like proteins, known to be involved in peroxide sensing in various organisms, strongly suggest that this $Zn(Cys)_4$ site is a distinctive feature of this class of peroxide regulators. Based on our structural data and the related *Pa*-Fur structure, we present a model of PerR which possesses a potential binding site for the regulatory metal and that may represent the active form of the protein that binds the DNA. Efforts are now directed at crystallizing the active protein and its DNA adduct.

Experimental procedures

Protein expression and purification

The *B. subtilis perR* gene was inserted between NdeI and XhoI restriction sites of pET-30c vector (Novagen). After sequence verification of each strand, the plasmid was introduced into *E. coli* BL21(DE3) competent cells (Sigma). The cells were grown aerobically at 37°C in 1 l of LB medium, containing 50 μg ml^{-1} kanamycin, until 0.6 OD at 600 nm. Production of PerR was induced by adding 1 mM IPTG, followed by 3 h incubation at 37°C. Cultures were then centrifuged at 5000 *g* for 10 min. From this point, all steps were performed at 4°C. Cells were resuspended in 30 ml of 100 mM Tris-HCl pH 8, 50 mM NaCl, 2 mM EDTA, 1 mM DTT (buffer A) prior to sonication. The cell lysate was then centrifuged for 30 min at 35 000 *g*. The resulting supernatant was directly loaded onto a MonoQ column (Amersham Biosciences). Proteins were eluted with a linear gradient of 0.05–1 M NaCl in buffer A. The fractions containing PerR were pooled and concentrated by ammonium sulphate precipitation (80%) at 4°C overnight. After centrifugation at 25 000 *g* for 45 min, the pellet was resuspended in 4 ml 100 mM Tris-HCl pH 8, 250 mM NaCl, 5 mM DTT and subjected to gel filtration using a Superdex-75 16/60 column (Amersham Biosciences). The fractions containing the dimeric protein were then collected and stored at −80°C. The concentration of PerR was calculated using an extinction coefficient of 9020 M^{-1} cm^{-1} at 277 nm.

Atomic absorption spectrometry

Prior to analysis, all the samples were buffer exchanged into Chelex-100 (Bio-Rad) treated 100 mM Tris-HCl pH 8. Buffer exchange was performed by using NAP-5 columns (Amersam Biosciences). The amount of zinc was determined by flame atomic absorption spectrometry (Perkin Elmer 560 Norwalk) using an external calibration curve. Mn^{2+} content of PerR-Zn-Mn was determined by electrothermal atomic absorption spectrometry (Hitachi 8270, Tokyo, Japan) using a Zeeman background correction and matrix matched external calibration curve.

Crystallization and structure determination

Screening of the crystallization conditions was initially performed with the TECAN robot using various commercial screens of Hampton Research and Qiagen. Crystals were obtained at 20°C with 20% PEG 6000, 1 M LiCl, and 0.1 M Tris-HCl pH 8 of the PEG–LiCl screen from Hampton Research. Crystals were then optimized and grown at 20°C from a 1:1 μl mixture of a 10 mg ml^{-1} protein solution (100 mM Tris-HCl, 250 mM NaCl, 5 mM DTT, 2 mM EDTA) with 25% PEG 6000, 1.5 M LiCl, 0.1 M Tris-HCl pH 8. For data collection, the crystals were transferred into a solution composed of the mother liquor and 25% glycerol as cryoprotectant.

PerR-Zn structure was determined using MAD X-ray diffraction data at 1.75 Å resolution collected around the Zn edge at 100 K on beam line FIP-BM30A (Roth *et al*., 2002) of the European Synchrotron Radiation Facility. Data reduction was performed with the xds program (Kabsch, 1993). The space group was P1 (a = 40.8 Å, b = 41.6 Å, c = 53.9 Å, α = 82.2°, β = 80.1°, γ = 60.9°) with potentially two molecules per asymmetric unit (solvent content of 50%). Two Zn atom sites were found with the solve program (Terwilliger and Berendzen, 1999) confirming the presence of two molecules in the asymmetric unit. After phase extension and solvent flattening with the resolve program (Terwilliger and Berendzen, 1999), the quality of the electron density map allowed the automated construction of 87 residues out of 288 (using resolve program). The model was completed manually with the coot molecular modelling package (Emsley and Cowtan, 2004). The refinement of this initial model was carried out with the Refmac5 program (Collaborative Computational Project, 1994) in the 30–1.75 Å resolution range without any NCS restraints. The final model contains residues His-4 to Asn-144 from monomer A and Ala-2 to Gly-145 from monomer B, both present in the asymmetric unit as well as 289 water molecules. The electron density is very well defined except for residues 49–53, 77–81 and 142–145 from monomer B located on a loop exposed to solvent. All residues fall within the allowed regions of the Ramachandran plot as defined by the procheck program (Laskowski *et al*., 1993). Statistics for all the data collections and refinement of the different structures are summarized in Table 1. The atomic co-ordinates and structure factors for PerR-Zn have been deposited into the PDB under the accession number 2FE3.

Protein oxidation and determination of the decomposition rate constants

Chemical reactions and FPLC analyses were performed with Chelex-100 treated buffers. Oxidative reactions were carried out at 37°C in 100 µl solution of 100 mM Tris-HCl pH 8, 500 mM NaCl, containing 20 µM of PerR-Zn in the presence of 100 eq. H_2O_2. For the reaction between PerR-Zn and diamide a 1/100 (protein/oxidant) ratio was also used. The samples were subjected to FPLC analysis using a gel filtration Superdex 75 HR10/30 analytical column (Amersham Biosciences) with a linear gradient of 100 mM Tris-HCl, 500 mM NaCl. The chromatograms were visualized and the different peaks were quantified using Unicorn software (Amersham Biosciences). The rate constant for the dimer decomposition was calculated by fitting the time evolution of the dimeric fraction to a one-phase exponential decay function.

DTNB titration of free thiols

The amount of thiol groups remaining in solution after exposure to H_2O_2 was determined by the Ellman's reagent (DTNB) using the E_{412nm} = 13 500 $M^{-1}cm^{-1}$ (calculated with B-mercaptoethanol). PerR (15 µM) was incubated with 100 eq. H_2O_2 for different times; reactions were stopped at different intervals by addition of 2 µl of HCl (1 M) into 10 µl reaction mixtures. Samples were neutralized by dilution (1:10) in a solution containing HEPES (1 M, pH 7.4) and DTNB (5 mM). Absorbance at 412 nm was immediately recorded.

Acknowledgements

We thank Josiane Arnaud for atomic absorption analyses, Christine Saint-Pierre for MALDI-TOF mass spectrometry measurements, David Lemaire for ESI-mass spectrometry analyses and Ludovic Champier for his help in cloning experiments during the initial stage of this work.

References

- *Barbirz, S., Jakob, U., and Glocker, M.O. (2000) Mass spectrometry unravels disulfide bond formation as the mechanism that activates a molecular chaperone. J Biol Chem 275: 18759–18766.*
  - CrossRef,
  - PubMed,
  - CAS,
  - Web of Science®
- *Barford, D. (2004) The role of cysteine residues as redox-sensitive regulatory switches. Curr Opin Struct Biol 14: 679–686.*
  - CrossRef,
  - PubMed,
  - CAS,
  - Web of Science®
- *Boylan, J.A., Posey, J.E., and Gherardini, F.C. (2003) Borrelia oxidative stress response regulator, BosR: a distinctive Zn-dependent transcriptional activator. Proc Natl Acad Sci USA 100: 11684–11689.*
  - CrossRef,
  - PubMed,
  - CAS,
  - Web of Science®,
  - ADS
- *Bsat, N., Herbig, A., Casillas-Martinez, L., Setlow, P., and Helmann, J.D. (1998) Bacillus subtilis contains multiple Fur homologues: identification of the iron uptake (Fur) and peroxide regulon (PerR) repressors. Mol Microbiol 29: 189–198.*

  Direct Link:

  - Abstract
  - Full Article (HTML)
  - PDF(715K)
  - References
  - Web of Science®
- *Chen, L., and Helmann, J.D. (1995) Bacillus subtilis MrgA is a Dps (PexB) homologue: evidence for metalloregulation of an oxidative-stress gene. Mol Microbiol 18: 295–300.*

  Direct Link:

  - Abstract
  - PDF(1826K)
  - Web of Science®
- *Chen, L., James, L.P., and Helmann, J.D. (1993) Metalloregulation in Bacillus subtilis: isolation and characterization of two genes differentially repressed by metal ions. J Bacteriol 175: 5428–5437.*
  - PubMed,
  - CAS,
  - Web of Science®
- *Chen, L., Keramati, L., and Helmann, J.D. (1995) Coordinate regulation of Bacillus subtilis peroxide stress genes by hydrogen peroxide and metal ions. Proc Natl Acad Sci USA 92: 8190–8194.*
  - CrossRef,
  - PubMed,
  - CAS,

    - Web of Science®,
    - ADS
- *Choi, H., Kim, S., Mukhopadhyay, P., Cho, S., Woo, J., Storz, G., and Ryu, S. (2001) Structural basis of the redox switch in the OxyR transcription factor. Cell 105: 103–113.*
    - CrossRef,
    - PubMed,
    - CAS,
    - Web of Science®
- *Collaborative Computational Project No. 4 (1994) The CCP4 suite: programs for protein crystallography. Acta Cryst D50: 760–763.*
- *Emsley, P., and Cowtan, K. (2004) Coot: model-building tools for molecular graphics. Acta Crystallogr D Biol Crystallogr 60: 2126–2132.*

  Direct Link:

    - Abstract
    - Full Article (HTML)
    - PDF(284K)
    - Web of Science®
- *Fuangthong, M., Herbig, A.F., Bsat, N., and Helmann, J.D. (2002) Regulation of the Bacillus subtilis fur and perR genes by PerR: not all members of the PerR regulon are peroxide inducible. J Bacteriol 184: 3276–3286.*
    - CrossRef,
    - PubMed,
    - CAS,
    - Web of Science®
- *Gonzalez de Peredo, A., Saint-Pierre, C., Adrait, A., Jacquamet, L., Latour, J.-M., Michaud-Soret, I., and Forest, E. (1999) Identification of the two zinc-bound cysteines in the ferric uptake regulation protein from Escherichia coli: chemical modification and mass spectrometry analysis. Biochemistry 38: 8582–8589.*
    - CrossRef,
    - PubMed,
    - CAS,
    - Web of Science®
- *Graumann, J., Lilie, H., Tang, X., Tucker, K.A., Hoffmann, J.H., Vijayalakshmi, J., et al. (2001) Activation of the redox-regulated molecular chaperone Hsp33: a two-step mechanism. Structure 9: 377–387.*
    - CrossRef,
    - PubMed,
    - CAS,
    - Web of Science®
- *Hahn, J.-S., Oh, S.-Y., Chater, K.F., Cho, Y.-H., and Roe, J.-H. (2000) H2O2-sensitive Fur-like repressor CatR regulating the major catalase gene in Streptomyces coelicolor. J Biol Chem 275: 38254–38260.*
    - CrossRef,
    - PubMed,
    - CAS,
    - Web of Science®
- *Herbig, A.F., and Helmann, J.D. (2001) Roles of metal ions and hydrogen peroxide in modulating the interaction of the Bacillus subtilis PerR peroxide regulon repressor with operator DNA. Mol Microbiol 41: 849–859.*

Direct Link:

- Abstract
- Full Article (HTML)
- PDF(1589K)
- References
- Web of Science®

- *Holm, L., and Sander, C. (1996) Mapping the protein universe. Science 273: 595–603.*
  - CrossRef,
  - PubMed,
  - CAS,
  - Web of Science®,
  - ADS
- *Horsburgh, M.J., Clements, M.O., Crossley, H., Ingham, E., and Foster, S.J. (2001) PerR controls oxidative stress resistance and iron storage proteins and is required for virulence in Staphylococcus aureus. Infect Immun 69: 3744–3754.*
  - CrossRef,
  - PubMed,
  - CAS,
  - Web of Science®
- *Huffman, J.L., and Brennan, R.G. (2002) Prokaryotic transcription regulators: more than just the helix-turn-helix motif. Curr Opin Struct Biol 12: 98–106.*
  - CrossRef,
  - PubMed,
  - CAS,
  - Web of Science®
- *Jacquamet, L., Aberdam, D., Adrait, A., Hazemann, J.-L., Latour, J.-M., and Michaud-Soret, I. (1998) X-ray absorption spectroscopy of a new zinc site in the Fur protein from Escherichia coli. Biochemistry 37: 2564–2571.*
  - CrossRef,
  - PubMed,
  - CAS,
  - Web of Science®
- *Jakob, U., Muse, W., Eser, M., and Bardwell, J.C. (1999) Chaperone activity with a redox switch. Cell 96: 341–352.*
  - CrossRef,
  - PubMed,
  - CAS,
  - Web of Science®
- *Jakob, U., Eser, M., and Bardwell, J.C. (2000) Redox switch of Hsp33 has a novel zinc binding motif. J Biol Chem 275: 38302–38310.*
  - CrossRef,
  - PubMed,
  - Web of Science®
- *Kabsch, W. (1993) Automatic processing of rotation diffraction data from crystals of initially unknown symmetry and cell constants. J Appl Cryst 26: 795–800.*

Direct Link:

- Abstract
- Full Article (HTML)
- PDF(665K)

    - Web of Science®
- *Kim, S.O., Merchant, K., Nudelman, R., Beyer, W.F. Jr, Keng, T., De Angelo, J., et al. (2002) OxyR: a molecular code for redox-related signaling. Cell 109: 383–396.*
    - CrossRef,
    - PubMed,
    - CAS,
    - Web of Science®
- *King, K.Y., Horenstein, J.A., and Caparon, M.G. (2000) Aerotolerance and peroxide resistance in peroxidase and PerR mutants of Streptococcus pyogenes. J Bacteriol 182: 5290–5299.*
    - CrossRef,
    - PubMed,
    - CAS,
    - Web of Science®
- *Laskowski, R.A., MacArthur, M.W., Moss, D.S., and Thornton, J.M. (1993) PROCHECK: a program to check the stereochemical quality of protein structures. J Appl Cryst 26: 283–291.*

  Direct Link:

    - Abstract
    - Full Article (HTML)
    - PDF(2256K)
    - Web of Science®
- *Lee, J.W., and Helmann, J.D. (2006) The PerR transcription factor senses H2O2 by metal-catalyzed histidine oxidation. Nature 440: 363–367.*
    - CrossRef,
    - PubMed,
    - CAS,
    - Web of Science®,
    - ADS
- *Mongkolsuk, S., and Helmann, J.D. (2002) Regulation of inducible peroxide stress responses. Mol Microbiol 45: 9–15.*

  Direct Link:

    - Abstract
    - Full Article (HTML)
    - PDF(82K)
    - References
    - Web of Science®
- *Ortiz de Orué Lucana, D., and Schrempf, H. (2000) The DNA-binding characteristics of the Streptomyces reticuli regulator FurS depend on the redox state of its cysteine residues. Mol Gen Genet 264: 341–353.*
    - CrossRef,
    - PubMed,
    - CAS
- *Paget, M.S., and Buttner, M.J. (2003) Thiol-based regulatory switches. Annu Rev Genet 37: 91–121.*
    - CrossRef,
    - PubMed,
    - CAS,

    - Web of Science®
- *Pohl, E., Holmes, R.K., and Hol, W.G. (1998) Motion of the DNA-binding domain with respect to the core of the diphtheria toxin repressor (DtxR) revealed in the crystal structures of apo- and holo-DtxR. J Biol Chem 273: 22420–22427.*
    - CrossRef,
    - PubMed,
    - CAS,
    - Web of Science®
- *Pohl, E., Holmes, R.K., and Hol, W.G. (1999a) Crystal structure of the iron-dependent regulator (IdeR) from Mycobacterium tuberculosis shows both metal binding sites fully occupied. J Mol Biol 285: 1145–1156.*
    - CrossRef,
    - PubMed,
    - CAS,
    - Web of Science®
- *Pohl, E., Holmes, R.K., and Hol, W.G. (1999b) Crystal structure of a cobalt-activated diphtheria toxin repressor-DNA complex reveals a metal-binding SH3-like domain. J Mol Biol 292: 653–667.*
    - CrossRef,
    - PubMed,
    - CAS,
    - Web of Science®
- *Pohl, E., Haller, J.C., Mijovilovich, A., Meyer-Klaucke, W., Garman, E., and Vasil, M.L. (2003) Architecture of a protein central to iron homeostasis: crystal structure and spectroscopic analysis of the ferric uptake regulator. Mol Microbiol 47: 903–915.*

  Direct Link:

    - Abstract
    - Full Article (HTML)
    - PDF(983K)
    - References
    - Web of Science®
- *Roth, M., Carpentier, P., Kaikati, O., Joly, J., Charrault, P., Pirocchi, M., et al. (2002) FIP: a highly automated beamline for multiwavelength anomalous diffraction experiments. Acta Cryst D58: 805–814.*
    - CAS
- *Schoneich, C. (2000) Mechanisms of metal-catalyzed oxidation of histidine to 2-oxo-histidine in peptides and proteins. J Pharm Biomed Anal 21: 1093–1097.*
    - CrossRef,
    - PubMed,
    - CAS,
    - Web of Science®
- *Simonson, T., and Calimet, N. (2002) Cys(x)His(y)-Zn^{2+} interactions: thiol versus thiolate coordination. Proteins 49: 37–48.*

  Direct Link:

    - Abstract
    - Full Article (HTML)
    - PDF(194K)
    - References

    - Web of Science® Times Cited: 35
- *Storz, G., and Imlay, J.A. (1999) Oxidative stress. Current Opinion Microbiol 2: 188–194.*
    - CrossRef,
    - PubMed,
    - Web of Science®
- *Terwilliger, T.C., and Berendzen, J. (1999) Automated structure solution for MIR and MAD. Acta Cryst D55: 849–861.*
- *Uchida, K., and Kawakishi, S. (1993) 2-Oxo-histidine as a novel biological marker for oxidatively modified proteins. FEBS Lett 332: 208–210.*
    - CrossRef,
    - PubMed,
    - CAS,
    - Web of Science®
- *Uchida, K., and Kawakishi, S. (1994) Identification of oxidized histidine generated at the active site of Cu,Zn-superoxide dismutase exposed to H2O2. Selective generation of 2-oxo-histidine at the histidine 118. J Biol Chem 269: 2405–2410.*
    - PubMed,
    - CAS,
    - Web of Science®
- *Van Vliet, A.H., Baillon, M.L., Penn, C.W., and Ketley, J.M. (1999) Campylobacter jejuni contains two Fur homologs: characterization of iron-responsive regulation of peroxide stress defense genes by the PerR repressor. J Bacteriol 181: 6371–6376.*
    - PubMed,
    - CAS,
    - Web of Science®
- *Zheng, M., Aslund, F., and Storz, G. (1998) Activation of the OxyR transcription factor by reversible disulfide bond formation. Science 279: 1718–1721.*
    - CrossRef,
    - PubMed,
    - CAS,
    - Web of Science®,
    - ADS
- *Zheng, M., Wang, X., Doan, B., Lewis, K.A., Schneider, T.D., and Storz, G. (2001a) Computation-directed identification of OxyR DNA binding sites in Escherichia coli. J Bacteriol 183: 4571–4579.*
    - CrossRef,
    - PubMed,
    - CAS,
    - Web of Science®
- *Zheng, M., Wang, X., Templeton, L.J., Smulski, D.R., LaRossa, R.A., and Storz, G. (2001b) DNA microarray-mediated transcriptional profiling of the Escherichia coli response to hydrogen peroxide. J Bacteriol 183: 4562–4570.*
    - CrossRef,
    - PubMed,
    - CAS,
    - Web of Science®

Supporting Information

FigS1. Purification of PerR-Zn. **FigS2.** Metal-dependent DNA binding of PerR-Zn. **FigS3.** Superposition of the N-terminal domains. **FigS4.** Superposition of PerR-Zn (orange) and *Pa*-Fur

(blue) dimerization domains. **FigS5.** CLUSTALW alignment of *Bs*-PerR with selected PerR-like proteins. **FigS6.** Model of the active PerR protein (for clarity only one monomer is represented).

Filename	Format	Size	Description
MMI5313FigsS1-S6.doc		736K	Supporting info item

Please note: Wiley-Blackwell is not responsible for the content or functionality of any supporting information supplied by the authors. Any queries (other than missing content) should be directed to the corresponding author for the article.

Get PDF (434K)

More content like this

Find more content:

- like this article

Find more content written by:

- Daouda A. K. Traoré
- Abdelnasser El Ghazouani
- Sougandi Ilango
- Jérôme Dupuy
- Lilian Jacquamet
- Jean-Luc Ferrer
- Christelle Caux-Thang
- Victor Duarte
- Jean-Marc Latour
- All Authors